High-Sensitivity of Self-Powered Gas Sensors Based on Piezoelectric Nanogenerators With Y-Doped 1-D ZnO Nanostructures

Yen-Lin Chu, Liang-Wen Ji, Jun-Hong Xie, and Tung-Te Chu

***Abstract*—In this work, yttrium-doped zinc oxide (Y-doped ZnO) nanorod (NR) arrays were grown using a simple facile hydrothermal solution route at low temperature to fabricate a self-powered gas sensor based on piezoelectric nanogenerator (PENG). The material properties of the 1-D NR arrays were observed using a field-emission scanning electron microscopy (FE-SEM) with an energy-dispersive X-ray (EDX), an X-ray diffraction (XRD), and a high-resolution transmission electron microscope (HR-TEM). The Y-doping concentration in the ZnO NRs was estimated to be 0.96 at%. Photoluminescence (PL) analysis was used to analyze the distribution of oxygen defects in the nanostructures. The Y-doped ZnO NRs were grown onto the bottom substrate and indium-tin-oxide polyethylene terephthalate (ITO-PET) substrates with silver (Ag) electrode were used as the top electrode to fabricate the PENG device. By introducing regular frequency mechanical external forces through a home-made impact system, the ZnO NRs of PENG devices generate piezoelectric effects, then the output electrical characteristics of PENGs were measured. It can be seen that the NRs with a Y-doping concentration of 7.5 mM showed a significant change in output voltage and current when exposed to carbon monoxide (CO) gas. Meanwhile, the Y:ZnO PENGs revealed remarkable sensitivity (58%) in 150 ppm CO environment. As a result, it was seen that such a device exhibited a self-powering characteristic and a significant sensitivity to CO gas. In the future, the device can also be combined with the Internet of Things (IoTs) for CO gas detection (e.g., portable gas sensors).**

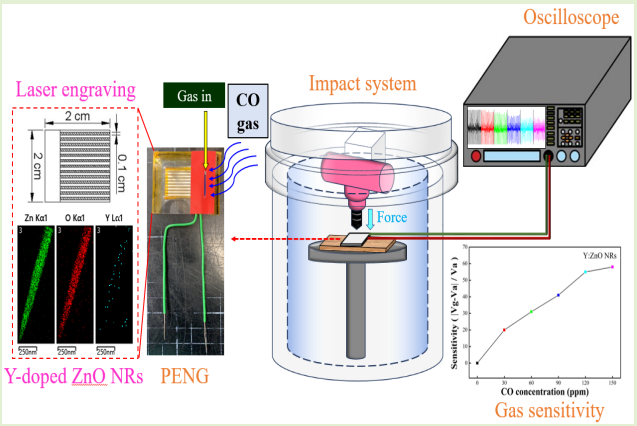

***Index Terms*—1-D nanorods (NRs), carbon monoxide (CO) gas, hydrothermal route, piezoelectric nanogenerator (PENG), yttrium dopant (Y-doped), zinc oxide (ZnO).**

I. Introduction

TRADITIONAL sensors usually rely on external power sources to operate. If the external power source space of the sensor can be removed and the sensor can self-supply power, the size of the sensor can be greatly reduced, the usage of the sensing devices will be more convenient [1]. This result aligns with the modern technology's demand for microsized devices and allows for more versatile usage of the sensor. The size and weight of the device are primarily influenced by the size of the battery. Through a self-powering system, natural mechanical energy such as tapping, knocking, impacting, pressure, vibration, flow, and sound wave, can be efficiently converted into electrical energy [2], [3]. This enables the realization of novel self-powered nanodevices without the need for external power supply. It can also address issues like low energy conversion efficiency in conditions such as solar panels that rely on sunlight for charging. Therefore, nanotechnology plays an extremely important role in self-powering research [4]. In the context of industrial development related to gases, the leakage of toxic gases poses an extremely important safety issue. By combining self-powering systems with gas sensors, workers can wear tiny sensing components to avoid the hazards of toxic gases in the environment.

Manuscript received 28 January 2024; revised 31 March 2024; accepted 10 April 2024. Date of publication 6 May 2024; date of current version 14 June 2024. This work was financially supported by the Ministry of Science and Technology of Taiwan under Contract MOST 110-2221-E-150-012-MY3. The associate editor coordinating the review of this article and approving it for publication was Dr. Chang-Soo Kim. *(Corresponding author: Liang-Wen Ji.)*

Yen-Lin Chu is with the Department of Central Engineering, Advanced Semiconductor Engineering, Inc., Kaohsiung 811, Taiwan, and also with the Institute of Electro-Optical and Materials Science, National Formosa University, Yunlin 632, Taiwan (e-mail: 10576123@gm.nfu.edu.tw).

Liang-Wen Ji is with the Institute of Electro-Optical and Materials Science, National Formosa University, Yunlin 632, Taiwan (e-mail: lwji@nfu.edu.tw).

Jun-Hong Xie is with the Department of Research and Development Center, EPISTAR Corporation, Inc., Hsinchu 300, Taiwan (e-mail: innewstylegg@gmail.com).

Tung-Te Chu is with the Department of Mechanical Automation Engineering, Kao Yuan University, Kaohsiung 821, Taiwan (e-mail: t30039@cc.kyu.edu.tw).

Digital Object Identifier 10.1109/JSEN.2024.3389931

Nanodevices show small size, lightweight, and portability, and it can become a new type of microwearable device [5].

Carbon monoxide (CO) is a common toxic gas that poses a threat to both humans and other organisms upon inhalation [6], [7], [8]. The environment is polluted by CO gas that is emitted due to human activity, and it destroys tropospheric ozone [9]. Furthermore, CO is a colorless, odorless, and nonirritating gas, hence, the necessity to develop sensors for detecting this gas [10], [11]. Hung et al. [12] used a ZnO thin films/self-assembled Au nanodots to prepare CO gas sensors. Shirage et al. [13] developed Sr- and Ni-doped ZnO nanostructure in CO gas sensor to overcome the difficulties with pure ZnO. Wang et al. [14] prepared silver (Ag)-modified ZnO flower-like microspheres for CO gas-sensing in 2021.

Currently, ZnO has been widely employed as an active sensing material for CO detection [15], [16], [17]. In general, ZnO belonging to the II–IV group is an n-type wide band gap semiconductor material [18]. The wurtzite crystal structure of ZnO is with the noncentrosymmetric hexagonal. ZnO material exhibit 3.2–3.4 eV of wide bandgap and 60 meV of high exciton binding energy at room temperature. Its lattice constants of a and c are 0.325 and 0.512 nm, respectively. Additionally, ZnO also reveals several advantages, for instance, excellent electron mobility, remarkable thermochemical characteristic, high mechanical strength, and nontoxicity [19], [20]. 1-D ZnO nanostructures, such as nanowires (NWs), nanobelts (NBs), nanotubes (NTs), nanoneedles (NNs), and nanorods (NRs) have been extensively used in recent years [21]. Many published works on the preparation of 1-D ZnO nanostructures can be roughly divided into two methods: vapor-phase deposition and liquid-phase deposition. Vapor-phase deposition methods include metal-organic chemical vapor deposition (MOCVD), vapor–solid (VS), pulse laser deposition (PLD), and high-temperature furnace [22], [23], [24]. Liquid-phase deposition methods include electrophoresis template method, chemical reduction, sonochemical way, and hydrothermal route method [25], [26], [27]. Among different production processes, hydrothermal route method is with three advantages: low temperature, cheap, and simple fabrication [28], [29]. ZnO materials can be employed in the fabrication of the novel electronic devices, such as gas sensors, solar cells, pH sensors, ultraviolet (UV) photodetectors (PDs), nanogenerators (NGs), photovoltaic devices, light-emitting diodes (LEDs), self-powered devices, humidity sensors, triboelectric generators, field emission (FE) emitters, and thin film transistors (TFTs) [30], [31], [32], [33], [34].

Yttrium (Y) is a rare-earth element that readily forms stable trivalent cations. According to relevant literature, the doping of Y in ZnO can result in a slight lattice distortion, but ZnO can still maintain its primary wurtzite crystal structure [35]. Formation energy analysis shows that the crystal energy is stable, and the increase in Y-doping concentration will improve the stability of the crystal structure, the Fermi level moves upward into the conduction band, showing n-type semiconductor characteristics [36]. In summary, we employed a hydrothermal method to fabricate a self-powered gas sensor based on Y-doped 1-D ZnO piezoelectric NG (PENG) in this study. The prepared methods of 1-D nanostructures, self-powered gas measurement systems, and gas-sensing mechanisms were presented in experimental and result section, and the 1-D ZnO samples with and without doped Y dopants were labeled Y:ZnO and ZnO PENGs, respectively.

II. Experimental Process and Device Measurement

A. Fabrication of Self-Powered Gas Sensors Based on PENGs With Y-Doped 1-D ZnO NR Arrays

As shown in Fig. 1(a), the device can divide two parts, one is top electrode and the other is 1-D nanostructures (bottom). An indium-tin-oxide (ITO) polyethylene terephthalate (PET) substrate (2 × 2 cm) was cut into square shape and laser engraving was used to define electrode pattern on the surface of ITO. Subsequently, a 100-nm thick Ag layer as an electrode was prepared and deposited using a radio frequency (RF) magnetron sputtering system. The power, target, and pressure of RF sputtering system were 50 W, pure 3-in Ag (99.99%), and 7.5×10^{-5} Torr, respectively. A hydrothermal route was employed in growing the 1-D ZnO NR arrays on the ITO/PET substrate. The sample was first deposited with a 100 nm ZnO seed layer using the RF magnetron sputtering system. The pressure, target, and power of RF system were 5.8×10^{-6} Torr, 3-in ZnO (99.99%), and 35 W, respectively. Subsequently, the hydrothermal growth way was carried out. All of the chemicals we used in the experiment were analytical reagent grade. Zinc nitrate hexahydrate [$Zn(NO_3)_2 \bullet 6H_2O$; 99.99%; 50 mM], hexamethylenetetramine ($C_6H_{12}N_4$, HMTA; 25 mM), and yttrium nitrate [$N_3O_9Y \bullet 6H_2O$; 99.99%; 7.5 mM] were mixed with the deionized (DI) water in glass beaker. When the solution is evenly stirred, the solution was transferred into serum bottle, and the sample was placed in it. The temperature and time of growth were 95 °C and 3 h, respectively. Finally, the top Ag electrode of ITO/PET and the Y-doped 1-D ZnO NR array (bottom) were tightly combined and heat-sealed to form a PENG, and then cut a hole near the conductor wire side for the gas inlet.

B. Sample Characterization and Electrical Measurement

The surface structures, material compositions, and atomic percentages of the samples with NR arrays were characterized by using FE scanning electron microscopy (FE-SEM, Hitachi S-4800I) with energy-dispersive X-ray (EDX) and elemental mapping. X-ray diffraction (XRD) technique [Bruker D8] with a monochromatic Cu Kα-1 radiation and high-resolution transmission electron microscope (HR-TEM, Philips Tecnai F20 G2 FEG-TEM) were used to study the crystalline property of NR samples. Photoluminescence (PL) spectrometer (Labram HR) with an excitation wavelength of 325 nm was used to examine optical performance of the 1-D ZnO and Y:ZnO NRs. On the other hand, the fabricated device was placed in the platform of a home-made impact system and connected to an external oscilloscope. The target gas (CO) was introduced into the system and adjusted to the desired gas concentration. The impact system was then activated to conduct electrical characteristic measurements of the sample. The electrical characteristics of

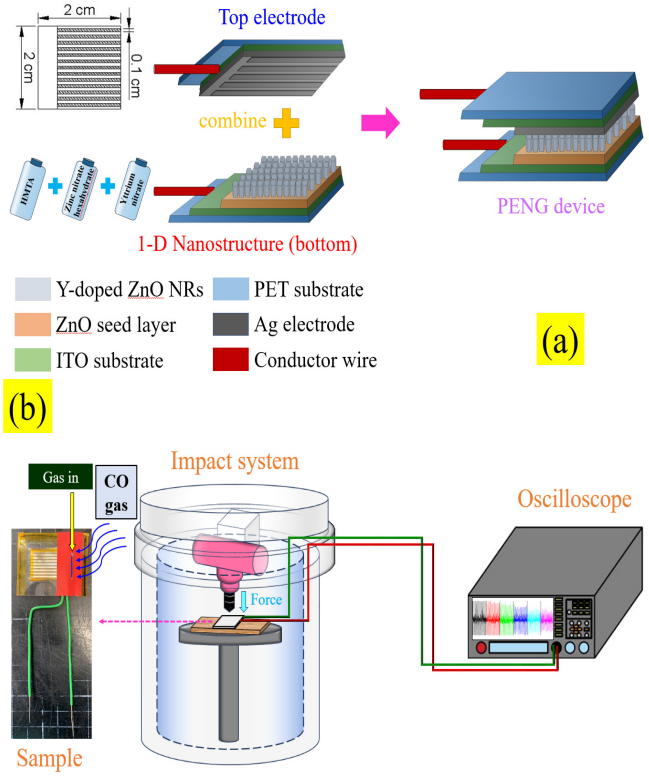

Fig. 1. (a) Schematic of the fabrication steps of PENGs with 1-D Y-doped ZnO NR arrays. (b) Electrical measurement with impact system for PENGs.

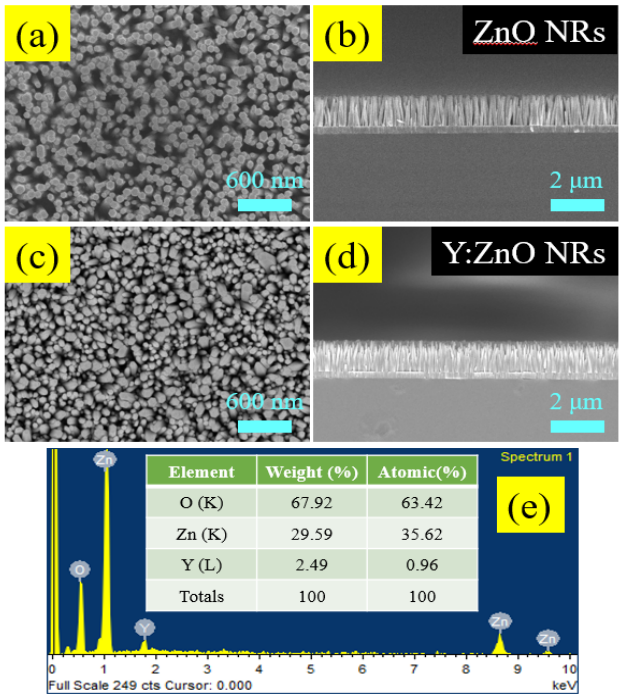

Fig. 2. (a) and (c) Top-view and (b) and (d) side-view FE-SEM images of the 1-D ZnO and Y:ZnO NR arrays. (e) EDX image of the 1-D Y:ZnO NRs.

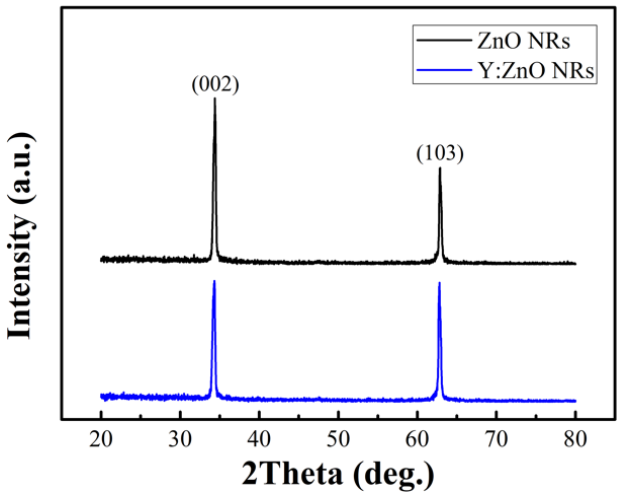

Fig. 3. XRD pattern measured from the as-grown 1-D ZnO and Y:ZnO NR samples.

all samples were evaluated by measuring the voltage–gas concentration (V–ppm), current–time (I–T) curve, and sensitivity. The external force and frequency provided by our impact system were 1.9 N and 13 Hz, respectively, as shown in Fig. 1(b).

III. Results and Discussion

A. Material Characteristics of 1-D ZnO and Y-Doped ZnO NR Arrays

The FE-SEM analysis results of the 1-D ZnO and Y:ZnO NR arrays are shown in Fig. 2. The top-view pictures reveal the as-grown nanostructures are with hexagonal structures. In addition, the cross-sectional view shows that all of the NRs are perpendicular to the substrates. The diameter and height of the ZnO NRs were approximately 109 nm and 1.33 μm, and the diameter and height of the Y:ZnO NRs were around 180 nm and 1.60 μm, respectively. This growth mechanism is attributed to differences in the release of crystal surface free energy due to the low ionization energy of Y element [37], as shown in Fig. 2(a)–(d). Fig. 2(e) exhibits the EDX spectrum of the Y:ZnO NRs, indicating that these NRs consist of Zn, O, and Y element. The respective Y content of the NR was 0.96 at%.

In Fig. 3 result, XRD analysis confirms the main peaks of hexagonal ZnO at (002) and (103) peaks [JCPDS Card No. 36-1451] [38], [39]. When Y element is doped into ZnO, no other peak positions generated, which confirms that the Zn ions during the growth of the NR can be replaced by Y ions, and also indicates that the lattice structure of the NR will not be changed after doping. At the same time, it was also found that the (002) and (103) peaks after doping slightly shift to the low phase angle. This reason means that the zinc ionic radius (0.074 nm) was lower than that of Y ionic radius (0.104 nm) [40].

Fig. 4 was obtained using HR-TEM to observe the nanostructure of yttrium-doped zinc oxide (Y-doped ZnO) NR arrays. In Fig. 4(a)–(c), TEM mapping analysis reveals that Zn (green), O (red), and Y (cyan) elements exist in a single 1-D ZnO NR, indicating Y dopant successfully doped into the ZnO NR. The selected area electron diffraction (SAED) pattern confirms that such a NR is with single-crystalline structure,

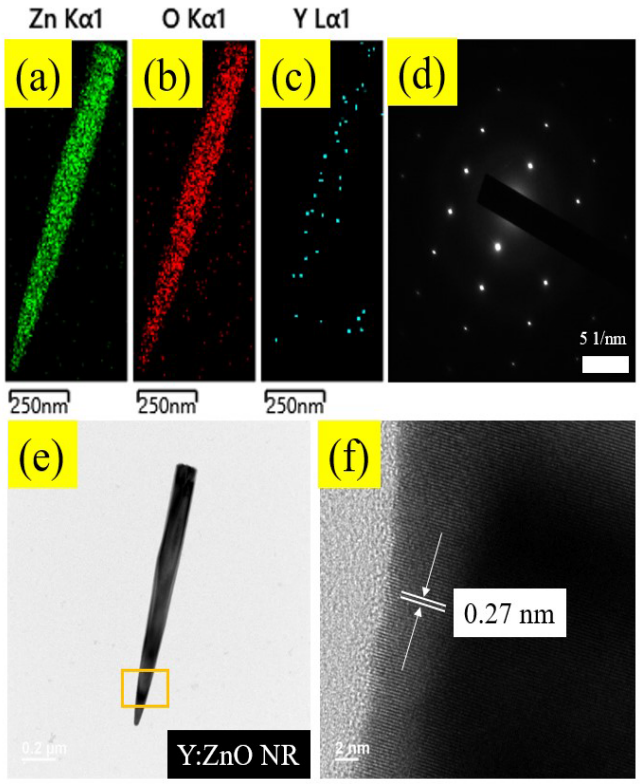

Fig. 4. (a)–(c) TEM elemental mapping images of the 1-D Y:ZnO NR. (d) SAED pattern of the Y:ZnO NR. (e) Low-magnification typical TEM result of a single 1-D Y:ZnO NR. (f) HR-TEM picture of the 1-D Y:ZnO NR.

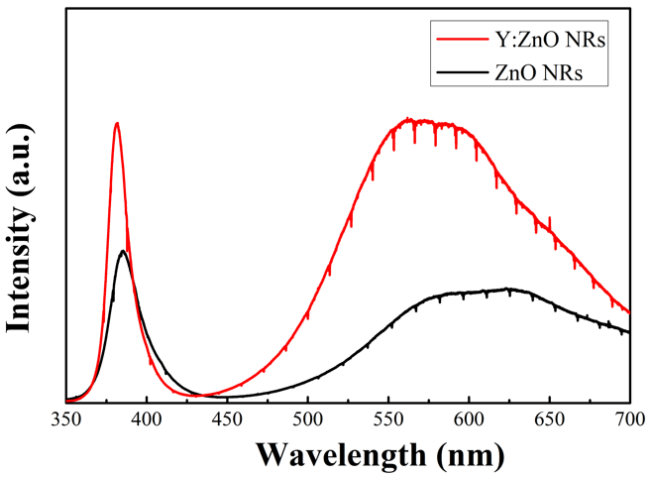

Fig. 5. PL spectrum of all NRs tested at room temperature.

as shown in Fig. 4(d). As seen in Fig. 4(e) and (f), a single NR with lattice spacing of 0.27 nm [orange rectangle], which aligns with the XRD analysis.

A PL spectrophotometer with a He–Cd laser (excitation wavelength was 325 nm) was used to measure and analyze the energy in the wavelength range of 350–700 nm [41], [42], [43]. Fig. 5 presents the PL analysis of the ZnO NRs with and without Y dopant. PL spectrum of ZnO was usually divided two regions: 1) UV emission region (~380 nm) and 2) green emission (~560 nm). 1) Shows free-excitonic transition recombination [near-band-edge (NBE) emission] and 2) reveals intrinsic defects or oxygen vacancies [deep-level emission (DLE)] [44], [45]. It was found that green emission of the Y:ZnO NRs has larger than that of the ZnO NRs. This phenomenon is attributed to Y ions can effectively replace Zn ions in 1-D NRs. Y-doping increases surface charge and reduces material bandgap, modifying the electrical properties of the material. The separation reaction of Y ions on the surface of the NR can promote the growth of vacancy in the nanostructure. Simultaneously, resulting in changes in the overall surface area of the NR and an increase in the number of defects [46].

B. Electrical Performances of All PENG Samples

A digital oscilloscope was employed in measuring the output voltage and current of the sample in this experiment. First, the PENG device was placed in a vacuum chamber and fixed on a platform, and the switch is turned on to impact such a device. The piezoelectric output voltage signals were transmitted to the oscilloscope through a conductor wire connecting on the same side of the device. The output current was converted through a simple voltage divider circuit. During the impact process, CO gas is introduced and the output voltage changes was recorded. The gas measurements were conducted in different CO gas concentrations: 0, 30, 60, 90, 120, and 150 ppm. No external voltage was applied to the device during the measurement.

Fig. 6 shows the electrical characteristic of two PENGs. The average output voltage values of the ZnO PENGs were 0.1848, 0.1934, 0.1803, 0.1763, 0.1798, and 0.1803 V at various concentrations (0, 30, 60, 90, 120, and 150 ppm, respectively) of CO gas. It can be seen that the average output voltage of ZnO has not clearly changed in CO condition. On the other hand, the average output voltages measured at different CO concentrations (0, 30, 60, 90, 120, and 150 ppm) of 7.5 mM Y-doped ZnO NR PENGs were 0.1603, 0.127, 0.111, 0.095, 0.072, and 0.067 V. By the above measured data, it can be found that the average output voltages of the devices were decreased with the increase of CO concentrations. In order to correctly understand that self-powered PENG can be used as a highly sensitive gas sensor, the sensitivities of the PENGs under various concentrations of CO gas should be defined. Similar to the traditional definition of the sensitivity of semiconductor gas sensors ($S\% = |Ra–Rg|/Ra \times 100\%$, where Ra and Rg depict the resistance of the sensor in air and test gas, respectively). The sensitivity of the self-powered CO sensor based on PENG can be simply illustrated as follows formula: $S\% = |Va–Vg|/Va \times 100\%$ [47], where Vg and Va denote the voltage of the device in CO gas and air gas, respectively. The sensitivities of the PENGs are increased with increasing CO gas concentration, as shown in Fig. 6 result. The sensitivity values of the ZnO PENG to CO gas were approximately 0% (0 ppm), 2% (30 ppm), 3% (60 ppm), 4% (90 ppm), 5% (120 ppm), and 5% (150 ppm). The sensitivity values of the Y:ZnO PENGs were about 0, 20, 31, 41, 55, and 58% for CO gas at 0, 30, 60, 90, 120, and 150 ppm, respectively. Compared with the ZnO PENGs, the Y:ZnO PENGs illustrated excellent sensitivity values under

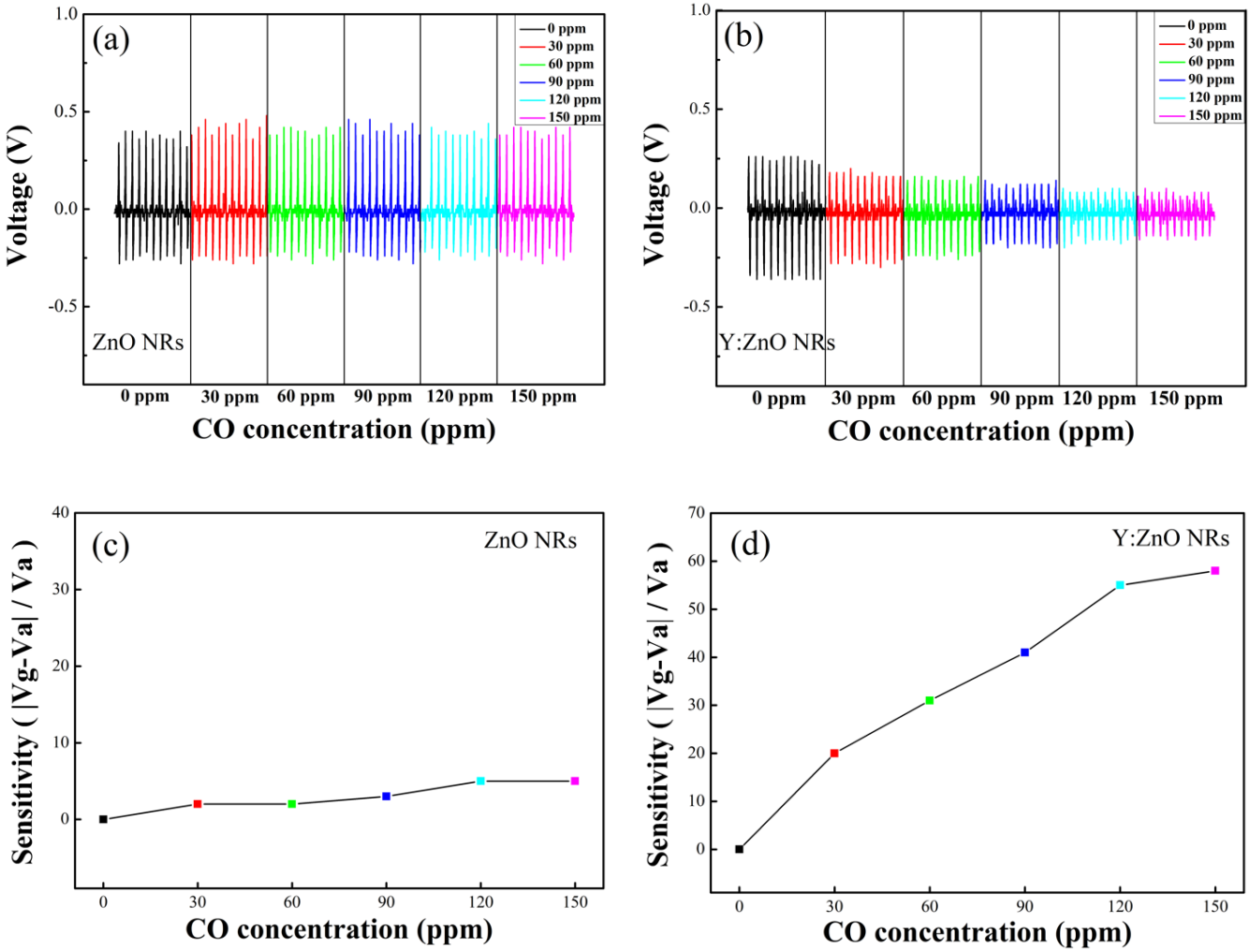

Fig. 6. (a) and (b) Average output voltage graph for ZnO and Y:ZnO NR samples in the presence of different CO gas concentrations. (c) and (d) Sensitivity of two samples in various CO gas concentrations.

TABLE I
COMPARISON ON PENG PERFORMANCE OF ZnO AND Y:ZnO NR

Material Sample	CO (ppm)	Voltage (V)	Sensitivity (%)
ZnO PENG	0	0.1848	0
	30	0.1934	2
	60	0.1803	3
	90	0.1763	4
	120	0.1798	5
	150	0.1803	5
Y:ZnO PENG	0	0.1603	0
	30	0.127	20
	60	0.111	31
	90	0.095	41
	120	0.072	55
	150	0.067	58

various CO gas concentrations, as revealed in Fig. 6(a)–(d) and Table I.

C. Gas-Sensing Mechanisms of All PENGs in Air and CO Gas

In order to explore the electrical characteristics of Y:ZnO PENG, it is necessary to understand the gas-sensing mechanism of such a device. Y dopant can be used to change the surface state and defect density of ZnO. The defect density will affect the gas adsorption rate onto the surface of the nanostructure, thereby leading to change the piezoelectric output voltages [48], [49]. As shown in Fig. 7, when the PENG device is exposed to CO gas with a reducing characteristic, the oxygen ions adsorbed on the surface of ZnO NRs will react with CO molecules and release the captured electrons flowing back into the conduction band of ZnO NRs. Such a process can increase the carrier density and reduce the thickness of the depletion layer in ZnO NRs. Hence, upon exposure to CO gas, the piezoelectric output voltage of the PENGs will be decreased due to the screen effect of free electrons [50], [51], [52].

When a nanostructure with piezoelectric characteristic undergoes tensile or compressive strain, an electric field is generated along the direction of the nanostructure. In the case of high electron concentration, some of the electrons will generate repulsive interactions, weakening the attraction between electrons and atoms [53], [54], [55]. When the screening effect is strong, the effective charge number will decrease, resulting in a decrease in the number of charges generated by the piezoelectric effect [56]. Therefore, some

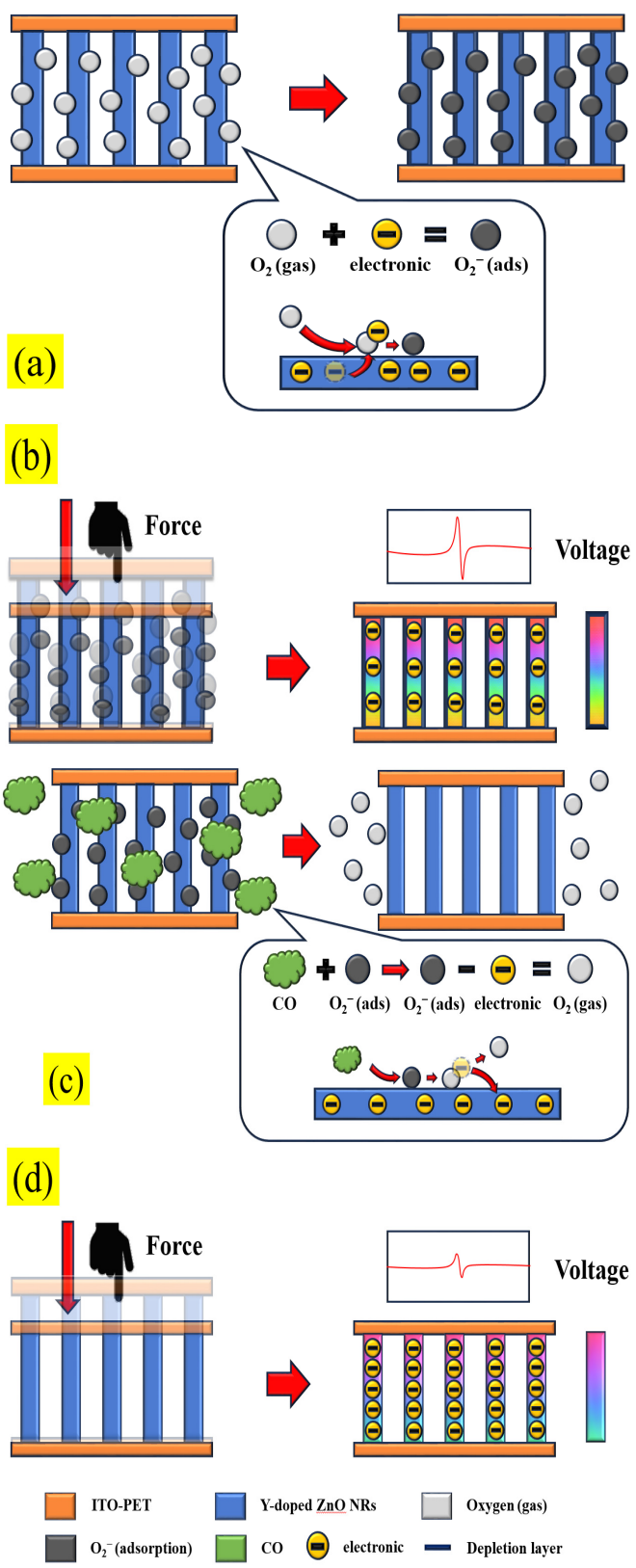

Fig. 7. (a) and (c) Schematic illustrates the impact of gas adsorption and desorption reactions on the direction of carrier movement and its effect on the output voltage in relation to the NRs. (b) and (d) Effect of NR carrier concentration on piezoelectric output in ambient atmosphere and reducing gas (CO).

of the charges inside the NRs are neutralized or suppressed, resulting in decreases at piezoelectric output voltage [57], [58],

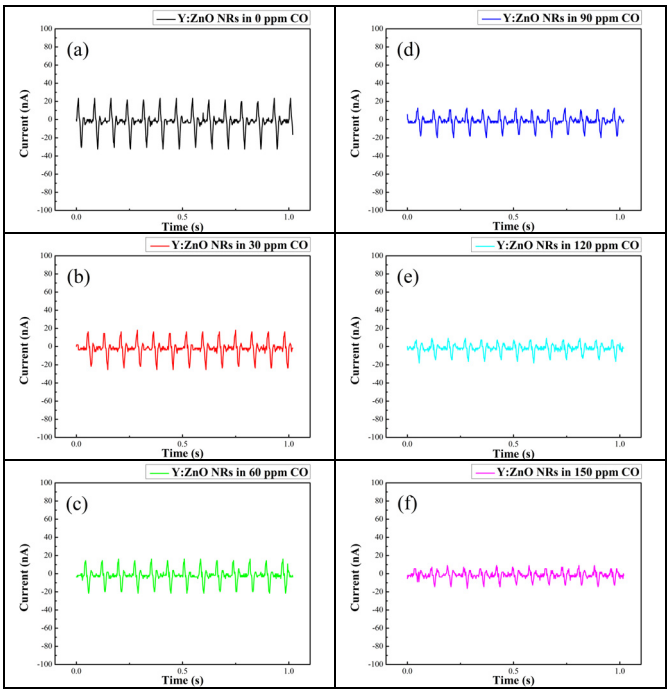

Fig. 8. (a)–(f) Average output current graph for Y:ZnO PENGs in the presence of various CO gas concentrations.

[59]. When the NR sample placed in air condition, surface vacancies adsorb oxygen molecules (O_2) in the atmosphere, and oxygen extracts electrons from the interior of the NR to form adsorbed negatively charged oxygen molecules (O_2^-), creating thick depletion layer and decrease carrier concertation. This phenomenon will affect the screening effect and increase the output voltage [60], [61]. Next, we introduce the reducing gas CO, which reacts with the adsorbed O_2^- on the surface. Under the oxygen reduction effect, O_2^- will be reduced by CO to O_2, generating CO_2 and e^-, and the reduced e^- will return to the conduction band of the ZnO NRs, causing increase in carrier concentration inside the NR and reduce the depletion layer of the NR. At this point, the piezoelectric output generated by applying compressive stress will be affected by the enhanced electric field screening effect after the carrier concentration increases [62], [63]. The internal charge of the NR is suppressed or neutralized due to the screening effect of the electric field, resulting in a decrease in the output voltage of the NR after introducing CO. The oxygen adsorbed on the 1-D ZnO NR sample surface undergoes the following reactions [64], [65], [66]:

$$O_{2\ (gas)} \rightarrow O2_{(ads)} \tag{1}$$

$$O_{2\ (gas)} + e^- \rightarrow O_{2\ (ads)}^- \tag{2}$$

$$O_{2\ (ads)}^- + 2CO_{(ads)} \rightarrow 2CO_2 + e^- \tag{3}$$

where (ads) indicates adsorbed. When Y is doped into the ZnO NR, Y^{3+} could replace the Zn^{2+} site, resulting in enlarging the crystal lattice interstice. In other words, the defect density of the surface of ZnO NRs will be increased due to the Y-doped in 1-D ZnO NRs [67], [68], [69], [70]. Therefore, the active sites of Y-doped ZnO compared to ZnO become more numerous,

TABLE II
COMPARISON ON DEVICE PERFORMANCE OF ZnO NANOMATERIALS IN LITERATURE

Material Sample	CO (ppm)	Sensitivity (%)	Temperature (℃)	Refs.
Al:ZnO	200	50	300	[76]
ZnO	200	90	300	[77]
Cu:ZnO	50	68	300	[78]
Al:ZnO	50	80	300	[79]
Pt:ZnO	20	48	300	[80]
Planar-type ZnO	200	74	400	[81]
ZnO	100	50	300	[82]
ZnO	150	5	Room temperature	This work
Y:ZnO	150	58	Room temperature	This work

which enhance the gas-sensing performance, as revealed in Fig. 7(a)–(d).

As shown in Fig. 8, a voltage divider circuit was configured for easily studying the current characteristic of the fabricated self-powered PENGs, where the output voltage is distributed to the resistance through the voltage divider circuit [71], [72]. An oscilloscope was used to measure the value of the piezoelectric output voltages and calculate the current through the formula: $V = I \times R$ [73], [74], [75]. The measured time was 1 s. The average output current of the 1-D Y:ZnO PENGs were around 19, 17, 15, 12, 9, and 6 nA to 0, 30, 60, 90, 120, and 150 ppm CO gas concentration, respectively. We found that piezoelectric output current was decreased while CO gas concentration was increased. The result is the same as output voltage in this work, as shown in Fig. 8(a)–(f).

The gas sensitivity characteristics of the ZnO NR arrays reported in previous studies [76], [77], [78], [79], [80], [81], [82] are summarized in Table II. Compared with the previously reports, the self-powered PENG devices with 1-D Y-doped ZnO NR arrays in this study has a remarkable sensitivity for CO gas.

IV. CONCLUSION

In summary, we demonstrated a self-powered gas sensor based on PENGs with Y-Doped 1-D ZnO NRs by using a simple hydrothermal method at low temperature, and it was triumphantly applied to enhance the gas sensitivity of the device. After FE-SEM result, HR-TEM pattern, and XRD image, it can be seen that the high-density 1-D NR arrays were successfully grown on the ZnO seed layer with single crystalline and preferentially grew in the *c*-axis direction with hexagonal characteristic. As revealed in EDX result, the Y-doping concentration in the 1-D ZnO nanostructures was estimated to be 0.96 at%. PL spectra showed the oxygen defect phenomenon with the increase of Y-doped concentration. The experimental results showed that the average output voltages of devices were decreased with different CO gas concentrations (0, 30, 60, 90, 120, and 150 ppm). This phenomenon is attributed to the increased oxygen vacancies in Y-doped ZnO nanostructures. Meanwhile, it was observed that the average current variation rate was decreased with increasing the CO gas concentration. As a result, it was also clearly to find that the performances of Y:ZnO PENGs with higher sensitivity are better than that of common ZnO PENGs. In general, most of the semiconductor gas sensors were employed in high temperatures. However, this investigation revealed that the fabricated self-powered gas sensors based on PENGs with excellent sensitivity can be operated at room temperature.

ACKNOWLEDGMENT

The authors would like to thank the Center for Micro/Nano Science and Technology, National Cheng Kung University, Tainan, Taiwan, for their assistance during the device characterization, and J. H. Xie for device fabrication and equipment support.

REFERENCES

[1] Z. L. Wang and J. Song, "Piezoelectric nanogenerators based on zinc oxide nanowire arrays," *Science*, vol. 312, no. 5771, pp. 242–246, Apr. 2006.
[2] X. Wang, J. Song, J. Liu, and Z. L. Wang, "Direct-current nanogenerator driven by ultrasonic waves," *Science*, vol. 316, no. 5821, pp. 102–105, Apr. 2007.
[3] Y.-L. Chu, S.-J. Young, L.-W. Ji, T.-T. Chu, and P.-H. Chen, "Synthesis of Ni-doped ZnO nanorod arrays by chemical bath deposition and their application to nanogenerators," *Energies*, vol. 13, no. 11, p. 2731, May 2020.
[4] C.-L. Hsu, I.-L. Su, and T.-J. Hsueh, "Sulfur-doped-ZnO-nanospire-based transparent flexible nanogenerator self-powered by environmental vibration," *RSC Adv.*, vol. 5, no. 43, pp. 34019–34026, 2015.
[5] S. Cui, Y. Zheng, T. Zhang, D. Wang, F. Zhou, and W. Liu, "Self-powered ammonia nanosensor based on the integration of the gas sensor and triboelectric nanogenerator," *Nano Energy*, vol. 49, pp. 31–39, Jul. 2018.
[6] J. Hang, Z. Luo, X. Wang, L. He, B. Wang, and W. Zhu, "The influence of street layouts and viaduct settings on daily carbon monoxide exposure and intake fraction in idealized urban canyons," *Environ. Pollut.*, vol. 220, pp. 72–86, Jan. 2017.
[7] G. Lippi, G. Rastelli, T. Meschi, L. Borghi, and G. Cervellin, "Pathophysiology, clinics, diagnosis and treatment of heart involvement in carbon monoxide poisoning," *Clin. Biochem.*, vol. 45, nos. 16–17, pp. 1278–1285, Nov. 2012.
[8] J. J. Rose et al., "Carbon monoxide poisoning: Pathogenesis, management, and future directions of therapy," *Amer. J. Respiratory Crit. Care Med.*, vol. 195, no. 5, pp. 596–606, Mar. 2017.
[9] I. O. Ribeiro et al., "Biomass burning and carbon monoxide patterns in Brazil during the extreme drought years of 2005, 2010, and 2015," *Environ. Pollut.*, vol. 243, pp. 1008–1014, Dec. 2018.
[10] D. D. Parrish et al., "Relationships between ozone and carbon monoxide at surface sites in the North Atlantic region," *J. Geophys. Res., Atmos.*, vol. 103, no. 11, pp. 13357–13376, Jun. 1998.
[11] A. Paliwal, A. Sharma, M. Tomar, and V. Gupta, "Carbon monoxide (CO) optical gas sensor based on ZnO thin films," *Sens. Actuators B, Chem.*, vol. 250, pp. 679–685, Oct. 2017.
[12] N. L. Hung, H. Kim, S.-K. Hong, and D. Kim, "Enhancement of CO gas sensing properties in ZnO thin films deposited on self-assembled Au nanodots," *Sens. Actuators B, Chem.*, vol. 151, no. 1, pp. 127–132, Nov. 2010.
[13] P. M. Shirage, A. K. Rana, Y. Kumar, S. Sen, S. G. Leonardi, and G. Neri, "Sr- and Ni-doping in ZnO nanorods synthesized by a simple wet chemical method as excellent materials for CO and CO_2 gas sensing," *RSC Adv.*, vol. 6, no. 86, pp. 82733–82742, 2016.
[14] Y. Wang, Y. Cui, X. Meng, Z. Zhang, and J. Cao, "A gas sensor based on Ag-modified ZnO flower-like microspheres: Temperature-modulated dual selectivity to CO and CH_4," *Surf. Inter.*, vol. 24, Jun. 2021, Art. no. 101110.
[15] W. Jigang, L. Ji, D. Yong, Z. Yan, M. Lihui, and H. Asadi, "Effect of platinum on the sensing performance of ZnO nanocluster to CO gas," *Solid State Commun.*, vols. 316–317, Aug. 2020, Art. no. 113954.
[16] M. Derakhshandeh and H. Anaraki-Ardakani, "A computational study on the experimentally observed sensitivity of Ga-doped ZnO nanocluster toward CO gas," *Phys. E, Low-Dimensional Syst. Nanostruct.*, vol. 84, pp. 298–302, Oct. 2016.

[17] S. Aslanzadeh, "Transition metal doped ZnO nanoclusters for carbon monoxide detection: DFT studies," *J. Mol. Model.*, vol. 22, no. 7, p. 160, Jun. 2016.

[18] Z. Zhou, W. Peng, S. Ke, and H. Deng, "Tetrapod-shaped ZnO whisker and its composites," *J. Mater. Process. Technol.*, vols. 89–90, pp. 415–418, May 1999.

[19] Y.-L. Chu et al., "Characteristics of gas sensors based on co-doped ZnO nanorod arrays," *J. Electrochemical Soc.*, vol. 167, no. 11, Jul. 2020, Art. no. 117503.

[20] Y.-L. Chu, S.-J. Young, L.-W. Ji, I.-T. Tang, and T.-T. Chu, "Fabrication of ultraviolet photodetectors based on Fe-doped ZnO nanorod structures," *Sensors*, vol. 20, no. 14, p. 3861, Jul. 2020.

[21] Y.-L. Chu, S.-J. Young, S.-H. Tsai, S. Arya, and T.-T. Chu, "High sensitivity of extended-gate field-effect transistors based on 1-D ZnO: Ag nanomaterials through a cheap photochemical synthesis as pH sensors at room temperature," *ACS Appl. Electron. Mater.*, vol. 6, no. 2, pp. 712–723, Jan. 2024.

[22] E. Chikoidze, M. Modreanu, V. Sallet, O. Gorochov, and P. Galtier, "Electrical properties of chlorine-doped ZnO thin films grown by MOCVD," *Phys. Status Solidi (A)*, vol. 205, no. 7, pp. 1575–1579, Jul. 2008.

[23] D. Wu et al., "Preparation and properties of Ni-doped ZnO rod arrays from aqueous solution," *J. Colloid Interface Sci.*, vol. 330, no. 2, pp. 380–385, Feb. 2009.

[24] R. Yousefi and B. Kamaluddin, "Dependence of photoluminescence peaks and ZnO nanowires diameter grown on silicon substrates at different temperatures and orientations," *J. Alloys Compounds*, vol. 479, nos. 1–2, pp. 11–14, Jun. 2009.

[25] M. Guo et al., "Effects of preparing conditions on the electrodeposition of well-aligned ZnO nanorod arrays," *Electrochimica Acta*, vol. 53, no. 14, pp. 4633–4641, May 2008.

[26] S. Jung, E. Oh, K. Lee, W. Park, and S. Jeong, "A sonochemical method for fabricating aligned ZnO nanorods," *Adv. Mater.*, vol. 19, no. 5, pp. 749–753, Mar. 2007.

[27] S.-J. Young and Y.-L. Chu, "Platinum nanoparticle-decorated ZnO nanorods improved the performance of methanol gas sensor," *J. Electrochemical Soc.*, vol. 167, no. 14, Nov. 2020, Art. no. 147508.

[28] Y. W. Wang, L. D. Zhang, G. Z. Wang, X. S. Peng, Z. Q. Chu, and C. H. Liang, "Catalytic growth of semiconducting zinc oxide nanowires and their photoluminescence properties," *J. Cryst. Growth*, vol. 234, no. 1, pp. 171–175, Jan. 2002.

[29] Y.-L. Chu, S.-J. Young, Y.-J. Chu, Y.-H. Liu, and T.-T. Chu, "High-performance UV photodetectors based on 1-D Ag/ZnO nanostructures with a simple photochemical process at room temperature," *IEEE Electron Device Lett.*, vol. 44, no. 1, pp. 124–127, Jan. 2023.

[30] S.-J. Young and Y.-L. Chu, "Hydrothermal synthesis and improved CH_3OH-sensing performance of ZnO nanorods with adsorbed Au NPs," *IEEE Trans. Electron Devices*, vol. 68, no. 4, pp. 1886–1891, Apr. 2021.

[31] Y.-L. Chu et al., "Improved pH-sensing characteristics by Pt nanoparticle-decorated ZnO nanostructures," *ECS J. Solid State Sci. Technol.*, vol. 10, no. 6, Jun. 2021, Art. no. 067001.

[32] Y.-L. Chu, S.-J. Young, R.-J. Ding, T.-T. Chu, T.-S. Lu, and L.-W. Ji, "Improving ZnO nanorod humidity sensors with Pt nanoparticle adsorption," *ECS J. Solid State Sci. Technol.*, vol. 10, no. 3, Mar. 2021, Art. no. 037003.

[33] Y.-L. Chu, S.-J. Young, L.-W. Ji, T.-T. Chu, and C.-H. Wu, "UV-enhanced field-emission performances of Pd-adsorbed ZnO nanorods through photochemical synthesis," *ECS J. Solid State Sci. Technol.*, vol. 10, no. 1, Jan. 2021, Art. no. 017001.

[34] S.-J. Young and Y.-L. Chu, "Characteristics of field emitters on the basis of Pd-adsorbed ZnO nanostructures by photochemical method," *ACS Appl. Nano Mater.*, vol. 4, no. 3, pp. 2515–2521, Mar. 2021.

[35] I. Atribak, A. Bueno-López, and A. García-García, "Role of yttrium loading in the physico-chemical properties and soot combustion activity of ceria and ceria–zirconia catalysts," *J. Mol. Catalysis A, Chem.*, vol. 300, nos. 1–2, pp. 103–110, Mar. 2009.

[36] M. Gao et al., "Enhancement of optical properties and donor-related emissions in Y-doped ZnO," *Superlatt. Microstruct.*, vol. 52, no. 1, pp. 84–91, Jul. 2012.

[37] S. Heo, Y. Lee, S. K. Sharma, S. Lee, and D. Y. Kim, "Mole-controlled growth of Y-doped ZnO nanostructures by hydrothermal method," *Current Appl. Phys.*, vol. 14, no. 11, pp. 1576–1581, Nov. 2014.

[38] Y.-L. Chu, S.-J. Young, D.-Y. Cai, and T.-T. Chu, "Characteristics of field-emission emitters based on graphene decorated ZnO nanostructures," *IEEE J. Electron Devices Soc.*, vol. 9, pp. 1076–1083, 2021.

[39] Y.-L. Chu et al., "Fabrication and characterization of UV photodetectors with Cu-doped ZnO nanorod arrays," *J. Electrochemical Soc.*, vol. 167, no. 2, Jan. 2020, Art. no. 027522.

[40] S. Anandan and S. Muthukumaran, "Influence of yttrium on optical, structural and photoluminescence properties of ZnO nanopowders by sol–gel method," *Opt. Mater.*, vol. 35, no. 12, pp. 2241–2249, Oct. 2013.

[41] C.-H. Huang, Y.-L. Chu, L.-W. Ji, I.-T. Tang, T.-T. Chu, and B.-J. Chiou, "Fabrication and characterization of homostructured photodiodes with Li-doped ZnO nanorods," *Microsyst. Technol.*, vol. 28, no. 1, pp. 369–375, Apr. 2020.

[42] S.-J. Young, Y.-H. Liu, Y.-L. Chu, and J.-Z. Huang, "Nonenzymatic glucose sensors of ZnO nanorods modified by Au nanoparticles," *IEEE Sensors J.*, vol. 23, no. 12, pp. 12503–12510, Jun. 2023.

[43] Y.-L. Chu et al., "Fabrication and characterization of Ni-doped ZnO nanorod arrays for UV photodetector application," *J. Electrochemical Soc.*, vol. 167, no. 6, Mar. 2020, Art. no. 067506.

[44] Y.-L. Chu, Y.-H. Liu, T.-T. Chu, and S.-J. Young, "Improved UV-sensing of Au-decorated ZnO nanostructure MSM photodetectors," *IEEE Sensors J.*, vol. 22, no. 6, pp. 5644–5650, Mar. 2022.

[45] Y.-L. Chu, S.-J. Young, T.-T. Chu, A. Khosla, K.-Y. Chiang, and L.-W. Ji, "Improvement of the UV-sensing performance of Ga-doped ZnO nanostructures via a wet chemical solution at room temperature," *ECS J. Solid State Sci. Technol.*, vol. 10, no. 12, Dec. 2021, Art. no. 127001.

[46] G. Turgut, S. Duman, and E. F. Keskenler, "The influence of Y contribution on crystallographic, topographic and optical properties of ZnO: A heterojunction diode application," *Superlatt. Microstruct.*, vol. 86, pp. 363–371, Oct. 2015.

[47] L. Xing et al., "Realizing room-temperature self-powered ethanol sensing of Au/ZnO nanowire arrays by coupling the piezotronics effect of ZnO and the catalysis of noble metal," *Appl. Phys. Lett.*, vol. 104, no. 1, Jan. 2014, Art. no. 013109.

[48] H. Guo, "Structure and optical properties of rare earth doped Y_2O_3 waveguide films derived by sol-gel process," *Thin Solid Films*, vol. 458, nos. 1–2, pp. 274–280, Jun. 2004.

[49] X. B. Li, Q. Q. Zhang, S. Y. Ma, G. X. Wan, F. M. Li, and X. L. Xu, "Microstructure optimization and gas sensing improvement of ZnO spherical structure through yttrium doping," *Sens. Actuators B, Chem.*, vol. 195, pp. 526–533, May 2014.

[50] X. Xue, Y. Nie, B. He, L. Xing, Y. Zhang, and Z. L. Wang, "Surface free-carrier screening effect on the output of a ZnO nanowire nanogenerator and its potential as a self-powered active gas sensor," *Nanotechnology*, vol. 24, no. 22, Apr. 2013, Art. no. 225501.

[51] G. Tian et al., "Understanding the potential screening effect through the discretely structured ZnO nanorods piezo array," *Nano Lett.*, vol. 20, no. 6, pp. 4270–4277, May 2020.

[52] P. Wang et al., "Synthesis of CdS nanorod arrays and their applications in flexible piezo-driven active H_2S sensors," *Nanotechnology*, vol. 25, no. 7, Jan. 2014, Art. no. 075501.

[53] Q. H. Li, Y. X. Liang, Q. Wan, and T. H. Wang, "Oxygen sensing characteristics of individual ZnO nanowire transistors," *Appl. Phys. Lett.*, vol. 85, no. 26, pp. 6389–6391, Dec. 2004.

[54] Z. Qu, Y. Fu, B. Yu, P. Deng, L. Xing, and X. Xue, "High and fast H_2S response of NiO/ZnO nanowire nanogenerator as a self-powered gas sensor," *Sens. Actuators B, Chem.*, vol. 222, pp. 78–86, Jan. 2016.

[55] Y. Fu, Y. Zhao, P. Wang, L. Xing, and X. Xue, "High response and selectivity of a Cu–ZnO nanowire nanogenerator as a self-powered/active H_2S sensor," *Phys. Chem. Chem. Phys.*, vol. 17, no. 3, pp. 2121–2126, 2015.

[56] R. K. Pandey, J. Dutta, S. Brahma, B. Rao, and C.-P. Liu, "Review on ZnO-based piezotronics and piezoelectric nanogenerators: Aspects of piezopotential and screening effect," *J. Phys., Mater.*, vol. 4, no. 4, Aug. 2021, Art. no. 044011.

[57] E. Kar, N. Bose, B. Dutta, S. Banerjee, N. Mukherjee, and S. Mukherjee, "2D SnO_2 nanosheet/PVDF composite based flexible, self-cleaning piezoelectric energy harvester," *Energy Convers. Manag.*, vol. 184, pp. 600–608, Mar. 2019.

[58] X. Wang, Y. Gao, Y. Wei, and Z. L. Wang, "Output of an ultrasonic wave-driven nanogenerator in a confined tube," *Nano Res.*, vol. 2, no. 3, pp. 177–182, Mar. 2009.

[59] C. Zhang et al., "Conjunction of triboelectric nanogenerator with induction coils as wireless power sources and self-powered wireless sensors," *Nature Commun.*, vol. 11, no. 1, pp. 1–10, Jan. 2020.

[60] M. Hjiri et al., "Effect of indium doping on ZnO based-gas sensor for CO," *Mater. Sci. Semicond. Process.*, vol. 27, pp. 319–325, Nov. 2014.

[61] J. H. Yu and G. M. Choi, "Selective CO gas detection of CuO- and ZnO-doped SnO_2 gas sensor," *Sens. Actuators B, Chem.*, vol. 75, nos. 1–2, pp. 56–61, Apr. 2001.
[62] S.-J. Jung and H. Yanagida, "The characterization of a CuO/ZnO heterocontact-type gas sensor having selectivity for CO gas," *Sens. Actuators B, Chem.*, vol. 37, nos. 1–2, pp. 55–60, Nov. 1996.
[63] M. Hjiri, F. Bahanan, M. S. Aida, L. El Mir, and G. Neri, "High performance CO gas sensor based on ZnO nanoparticles," *J. Inorganic Organometallic Polym. Mater.*, vol. 30, no. 10, pp. 4063–4071, Apr. 2020.
[64] A. M. Pineda-Reyes, M. R. Herrera-Rivera, H. Rojas-Chávez, H. Cruz-Martínez, and D. I. Medina, "Recent advances in ZnO-based carbon monoxide sensors: Role of doping," *Sensors*, vol. 21, no. 13, p. 4425, Jun. 2021.
[65] C. Wang, Y. Li, F. Gong, Y. Zhang, S. Fang, and H. Zhang, "Advances in doped ZnO nanostructures for gas sensor," *Chem. Rec.*, vol. 20, no. 12, pp. 1553–1567, Dec. 2020.
[66] Y. Luo et al., "Role of cobalt in co-ZnO nanoflower gas sensors for the detection of low concentration of VOCs," *Sens. Actuators B, Chem.*, vol. 360, Jun. 2022, Art. no. 131674.
[67] P. Yu, J. Wang, H.-Y. Du, P.-J. Yao, Y. Hao, and X.-G. Li, "Y-doped ZnO nanorods by hydrothermal method and their acetone gas sensitivity," *J. Nanomaterials*, vol. 2013, pp. 1–6, Dec. 2013.
[68] T. Minami, T. Yamamoto, and T. Miyata, "Highly transparent and conductive rare earth-doped ZnO thin films prepared by magnetron sputtering," *Thin Solid Films*, vol. 366, nos. 1–2, pp. 63–68, May 2000.
[69] W. C. Lee et al., "An enhanced gas ionization sensor from Y-doped vertically aligned conductive ZnO nanorods," *Sens. Actuators B, Chem.*, vol. 237, pp. 724–732, Dec. 2016.
[70] Y.-T. Tsai et al., "High sensitivity of NO gas sensors based on novel Ag-doped ZnO nanoflowers enhanced with a UV light-emitting diode," *ACS Omega*, vol. 3, no. 10, pp. 13798–13807, Oct. 2018.
[71] N. Sheikh, N. Afzulpurkar, and M. W. Ashraf, "Robust nanogenerator based on vertically aligned ZnO nanorods using copper substrate," *J. Nanomaterials*, vol. 2013, pp. 1–8, Oct. 2013.
[72] Y. Xi, D. H. Lien, R. S. Yang, C. Xu, and C. G. Hu, "Direct-current nanogenerator based on ZnO nanotube arrays," *Phys. Status Solidi (RRL)*, vol. 5, no. 2, pp. 77–79, Jan. 2011.
[73] K.-T. Lam, Y.-L. Chu, L.-W. Ji, Y.-J. Hsiao, T.-T. Chu, and B.-W. Huang, "Characterization of nanogenerators based on S-doped zinc oxide nanorod arrays," *Microsyst. Technol.*, vol. 28, no. 1, pp. 395–401, May 2020.
[74] Y.-L. Chu, S.-J. Young, H.-C. Chang, S. Arya, Y.-H. Liu, and T.-T. Chu, "Enhanced nanogenerator performances of 1-D Al-doped ZnO nanorod arrays through ultrasonic wave systems," *ACS Appl. Electron. Mater.*, vol. 5, no. 2, pp. 1277–1285, Feb. 2023.
[75] Y.-L. Chu, R.-J. Ding, T.-T. Chu, and S.-J. Young, "UV-enhanced electrical performances of ZnO:Ga nanostructure nanogenerators by using ultrasonic waves," *IEEE Trans. Electron Devices*, vol. 69, no. 10, pp. 5800–5807, Oct. 2022.
[76] J. Chang, H. H. Kuo, I. C. Leu, and M. H. Hon, "The effects of thickness and operation temperature on ZnO:Al thin film CO gas sensor," *Sens. Actuators B, Chem.*, vol. 84, no. 2, pp. 258–264, 2002.
[77] T. Krishnakumar et al., "CO gas sensing of ZnO nanostructures synthesized by an assisted microwave wet chemical route," *Sens. Actuators B, Chem.*, vol. 143, no. 1, pp. 198–204, Dec. 2009.
[78] H. Gong, J. Q. Hu, J. H. Wang, C. H. Ong, and F. R. Zhu, "Nano-crystalline cu-doped ZnO thin film gas sensor for CO," *Sens. Actuators B, Chem.*, vol. 115, no. 1, pp. 247–251, May 2006.
[79] M. Hjiri, L. El Mir, S. G. Leonardi, A. Pistone, L. Mavilia, and G. Neri, "Al-doped ZnO for highly sensitive CO gas sensors," *Sens. Actuators B, Chem.*, vol. 196, pp. 413–420, Jun. 2014.
[80] G. E. Buono-Core, A. H. Klahn, G. Cabello, and L. Lillo, "Characterization of amorphous Pt/ZnO films grown on silicon(100) substrates by a photochemical metal organic deposition and their potential use as gas sensors," *Polyhedron*, vol. 62, pp. 1–6, Oct. 2013.
[81] N. D. Khoang et al., "On-chip growth of wafer-scale planar-type ZnO nanorod sensors for effective detection of CO gas," *Sens. Actuators B, Chem.*, vol. 181, pp. 529–536, May 2013.
[82] S. K. Lim, S.-H. Hwang, S. Kim, and H. Park, "Preparation of ZnO nanorods by microemulsion synthesis and their application as a CO gas sensor," *Sens. Actuators B, Chem.*, vol. 160, no. 1, pp. 94–98, Dec. 2011.

Yen-Lin Chu was born in Kaohsiung, Taiwan, in 1991. He received the Ph.D. degree from the Department of Electro-Optical Engineering and the Institute of Electro-Optical and Materials Science, National Formosa University, Yunlin, Taiwan, in 2021.

He is currently a Supervisor at the Department of Central Engineering, Advanced Semiconductor Engineering (ASE), Inc., Kaohsiung. His current research interests include nanotechnology system, semiconductor manufacture, optoelectronic device, novel energy material, growth of semiconductor nanostructure, artificial intelligence (AI) application, low carbon material evaluation, IC package, and test.

Liang-Wen Ji was born in Taipei City, Taiwan, in 1965. He received the B.S. degree in physics, the M.S. degree in material science, and the Ph.D. degree in electrical engineering from National Cheng Kung University, Tainan, Taiwan, in 1988, 1990, and 2004, respectively.

In 2005, Dr. Ji joined the Institute of Electro-Optical and Materials Science/ Department of Electro-Optical Engineering, National Formosa University, Yunlin, Taiwan, as an Associate Professor, and also served as the Director of the Research and Development Center for Display Technologies. He was promoted to a Full Professor in 2007 and has been a Distinguished Professor at National Formosa University since 2019. His current research interests include semiconductor physic, optoelectronic, nanotechnology, and Artificial Intelligence of Thing (AIoT) technology.

Dr. Ji has been a Fellow of the Taiwanese Institute of Knowledge Innovation (TIKI) since 2014. He was elected as a Fellow of the Institution of Engineering and Technology (IET) in 2023. He was a recipient of the Research Award from Lam Research Taiwan Company Ltd., Taiwan, in 2004.

Jun-Hong Xie was born in Tainan, Taiwan, in 1998. He received the M.S. degree from the Institute of Electro-Optical and Materials Science, National Formosa University, Yunlin, Taiwan, in 2023.

He is currently a Senior Engineer at the Department of Research and Development Center, EPISTAR Corporation Inc., Hsinchu, Taiwan. His research interests include optoelectronic device with wide bandgap semiconductor and 1-D nanostructure.

Tung-Te Chu was born in Nantou, Taiwan, in 1958. He received the Ph.D. degree in optoelectronic engineering from Changchun University of Science and Technology, Changchun, Mainland China, in 2010, and the another Ph.D. degree in technology of engineering from the National Kaohsiung First University of Science and Technology, Kaohsiung, Taiwan, in 2012.

He is currently an Assistant Professor with Kao Yuan University, Kaohsiung. His current research interests include semiconductor device, mechanical engineering, novel energy material, artificial intelligence (AI) application, quality management, and precision mechanical sensing device.